Design of a Multi-Wavelength Fiber Laser Based on Tm:Er:Yb:Ho Co-Doped Germanate Glass

Mario Christian Falconi, *Student Member, IEEE*, Dario Laneve, Vincenza Portosi, Stefano Taccheo, and Francesco Prudenzano

***Abstract*—In this article, for the first time, an efficient multi-wavelength fiber laser based on a Tm:Er:Yb:Ho co-doped germanate glass, optically pumped at 980 nm wavelength and simultaneously emitting at 1550 nm, 1800 nm and 2050 nm wavelengths, is designed and optimized. An exhaustive model, taking into account the energy transfer phenomena between different rare earths, is developed. The device behavior is investigated by means of several parametric sweeps with respect to the input pump power, the fiber length, the dopant concentrations and the output mirrors reflectivities. Four optimal concentrations have been found by means of a home-made computer code based on particle swarm optimization (PSO) approach, allowing a global solution search. These concentrations allow levels of output powers very close to each other, equal to 20 mW $\pm$ 0.1% at 1550 nm, 1800 nm and 2050 nm, respectively. These results predict the possibility of tailoring the dopant concentrations in order to construct broadband optical sources with similar emission powers at multiple wavelengths and broadband amplifiers.**

***Index Terms*—Erbium, fiber laser, germanate glass, holmium, multi-wavelength lasing, thulium, ytterbium.**

I. Introduction

IN RECENT years, novel optical fiber amplifiers and lasers providing multi-wavelength laser emission and broadband signal amplification in the wavelength range $\lambda = 1.5\,\mu$m to $2.2\,\mu$m have attracted a lot of interest. This is due to the wide range of potential applications which include, but are not limited to, optical communications systems, remote sensing, spectroscopy, environmental monitoring and medicine [1]–[12]. There are several glasses which can be exploited for making lasers and amplified spontaneous emission (ASE) sources operating at these wavelengths, such as silicate, chalcogenide, antimony, fluorophosphate and germanate glasses. In particular, germanate glass exhibits a number of interesting properties: i) higher refractive index than fused silica ($n \approx 1.9$), ii) broad optical transmission window up to about $\lambda = 5\,\mu$m, iii) relatively high glass transition temperature ($T_g \approx 400\,^\circ$C), iv) high physicochemical stability (especially with respect to fluoride glass), v) high rare-earth-ion solubility (with respect to chalcogenide glass), vi) low phonon energy, vii) rather low probability of non-radiative relaxation [4], [11]. However, glasses doped with several rare earths exhibit a high number of spectroscopic parameters, due to the presence of energy transfer phenomena among different rare earth ions. Moreover, the nonlinear nature of such phenomena, which vary with the dopant concentration levels, makes the design of optical devices doped with multiple rare earths not trivial.

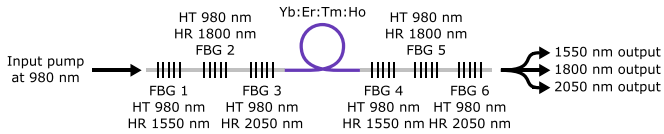

Fig. 1. Schematic of the device.

In this paper, for the first time to the best of our knowledge, a multi-wavelength fiber laser exploiting an Tm:Er:Yb:Ho co-doped germanate glass fiber pumped at $\lambda_p = 980$ nm is designed and refined via a global search approach. Experimental data reported in literature are employed in the simulations, in particular for the spectroscopic and optical parameters. Fig. 1 shows the schematic of the device. The optical cavity is composed of three couples of high reflective (HR) fiber Bragg gratings, i.e. three input mirrors and three output mirrors, which allow simultaneous laser emission at $\lambda_{s1} = 1550$ nm, $\lambda_{s2} = 1800$ nm and $\lambda_{s3} = 2050$ nm. This configuration exhibits both low cost (only one laser diode is needed for pumping) and high compactness (only one active medium is needed). Moreover it shows that, in principle, wideband amplification and multi-wavelengh laser emission can be finely tailored in a single fiber via a proper choice of the different dopant concentrations. This suggest, as a consequence, the feasibility of ultrashort pulse emission which is of interest in many fields of application.

II. Tm:Er:Yb:Ho Laser Model

The model of the Tm:Er:Yb:Ho rare earth system, optically pumped at $\lambda_p = 980$ nm, includes a total of 11 energy levels [9],

Manuscript received October 22, 2019; revised November 24, 2019; accepted January 6, 2020. Date of publication January 16, 2020; date of current version April 15, 2020. This work was supported in part by POR FESR-FSE 2014-2020 Innonetwork "Sinach – Integrated systems for mininvasive surgical navigation" – under Grant BLNGWP7, in part by PON R&I 2014-2020 "New Satellites Generation components - NSG" – under Grant ARS01_01215 NSG. *(Corresponding author: Francesco Prudenzano.)*

M. C. Falconi, D. Laneve, V. Portosi, and F. Prudenzano are with the Department of Electrical and Information Engineering, Politecnico di Bari, 70125 Bari, Italy (e-mail: mariochristian.falconi@poliba.it; dario.laneve@poliba.it; vincenza.portosi@poliba.it; francesco.prudenzano@poliba.it).

S. Taccheo is with the Laser Group, Swansea University, SA2 8PP Swansea, United Kingdom, and also with the Department of Electronics and Telecommunications, Politecnico di Torino, 10129 Torino, Italy (e-mail: s.taccheo@swansea.ac.uk).

Color versions of one or more of the figures in this article are available online at https://ieeexplore.ieee.org.

Digital Object Identifier 10.1109/JLT.2020.2966999

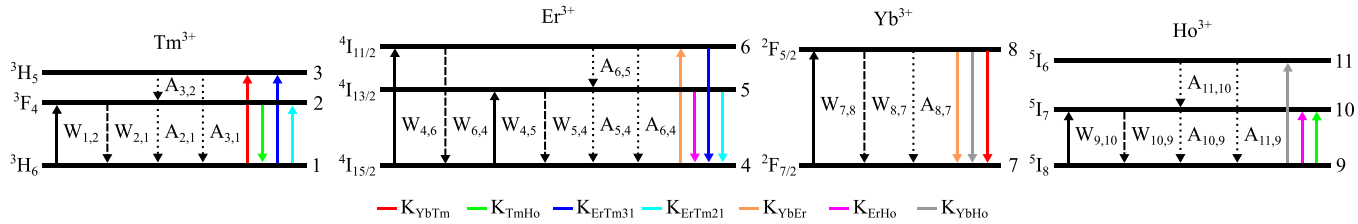

Fig. 2. Energy levels diagram.

as follows: i) $^4I_{15/2}$, $^4I_{13/2}$ and $^4I_{11/2}$ for the erbium ions; ii) $^2F_{7/2}$ and $^2F_{5/2}$ for the ytterbium ions; iii) $^3H_6$, $^3F_4$ and $^3H_5$ for the thulium ions; iv) $^5I_8$, $^5I_7$ and $^5I_6$ for the holmium ions. All indicated levels are manifolds and the spectral overlapping of the manifolds is considered in the model via cumulative energy transfer constants. Higher energy levels are not considered here, since the interactions with the considered set of levels are negligible. This is due to energy mismatch and/or extremely low excited-state transition probability due to low populations of starting levels. The energy levels scheme is shown in Fig. 2.

Due to the presence of several rare earth ions, in addition to the typical phenomena of absorption and stimulated/spontaneous emission, it is mandatory to consider the energy transfer phenomena occurring between different pairs of ions. The mechanism of energy transfer among the four rare earths is very complex, involving several transitions. As an example, the population inversion for 1800 nm emission, with reference to Yb^{3+}-Tm^{3+} interaction, is obtained as follows: i) at first, Yb^{3+} ions are excited to the $^2F_{5/2}$ level under 980 nm optical pumping, ii) these ions can relax radiatively to the $^2F_{7/2}$ ground level or partially transfer energy to the $^3H_5$ level of Tm^{3+} ions by a phonon-assisted energy transfer (PAET); iii) the energy gap between $^3H_5$ and $^3F_4$ multiplets of Tm^{3+} ions leads to fast population of $^3F_4$ metastable level by multi-phonon relaxation (MPR) [5]. In the model, this is taken into account via the energy transfer parameter K_{YbTm} and the decay rate $A_{3,2}$. Similarly, all the other interactions are considered.

By using a rate equations approach [13]–[19] and neglecting amplified spontaneous emission (ASE), the following system for the energy level populations $N_1, N_2, \ldots, N_{11}$ is written:

$$\frac{\partial N_{11}}{\partial t} = -A_{11,10}N_{11} - A_{11,9}N_{11} + K_{\mathrm{YbHo}}N_8N_9 \tag{1a}$$

$$\frac{\partial N_{10}}{\partial t} = W_{9,10}N_9 - W_{10,9}N_{10} - A_{10,9}N_{10} + A_{11,10}N_{11} + K_{\mathrm{ErHo}}N_5N_9 + K_{\mathrm{TmHo}}N_2N_9 \tag{1b}$$

$$\frac{\partial N_9}{\partial t} = -W_{9,10}N_9 + W_{10,9}N_{10} + A_{10,9}N_{10} + A_{11,9}N_{11} - K_{\mathrm{YbHo}}N_8N_9 - K_{\mathrm{ErHo}}N_5N_9 - K_{\mathrm{TmHo}}N_2N_9 \tag{1c}$$

$$\frac{\partial N_8}{\partial t} = W_{7,8}N_7 - W_{8,7}N_8 - A_{8,7}N_8 - K_{\mathrm{YbEr}}N_4N_8 - K_{\mathrm{YbHo}}N_8N_9 - K_{\mathrm{YbTm}}N_1N_8 \tag{1d}$$

$$\frac{\partial N_7}{\partial t} = -W_{7,8}N_7 + W_{8,7}N_8 + A_{8,7}N_8 + K_{\mathrm{YbEr}}N_4N_8 + K_{\mathrm{YbHo}}N_8N_9 + K_{\mathrm{YbTm}}N_1N_8 \tag{1e}$$

$$\frac{\partial N_6}{\partial t} = W_{4,6}N_4 - W_{6,4}N_6 - A_{6,5}N_6 - A_{6,4}N_6 + K_{\mathrm{YbEr}}N_4N_8 - K_{\mathrm{ErTm31}}N_1N_6 \tag{1f}$$

$$\frac{\partial N_5}{\partial t} = W_{4,5}N_4 - W_{5,4}N_5 + A_{6,5}N_6 - A_{5,4}N_5 - K_{\mathrm{ErHo}}N_5N_9 - K_{\mathrm{ErTm21}}N_1N_5 \tag{1g}$$

$$\frac{\partial N_4}{\partial t} = -W_{4,6}N_4 + W_{6,4}N_6 - W_{4,5}N_4 + W_{5,4}N_5 + A_{6,4}N_6 + A_{5,4}N_5 - K_{\mathrm{YbEr}}N_4N_8 + K_{\mathrm{ErHo}}N_5N_9 + K_{\mathrm{ErTm31}}N_1N_6 + K_{\mathrm{ErTm21}}N_1N_5 \tag{1h}$$

$$\frac{\partial N_3}{\partial t} = -A_{3,2}N_3 - A_{3,1}N_3 + K_{\mathrm{YbTm}}N_1N_8 + K_{\mathrm{ErTm31}}N_1N_6 \tag{1i}$$

$$\frac{\partial N_2}{\partial t} = W_{1,2}N_1 - W_{2,1}N_2 + A_{3,2}N_3 - A_{2,1}N_2 - K_{\mathrm{TmHo}}N_2N_9 + K_{\mathrm{ErTm21}}N_1N_5 \tag{1j}$$

$$\frac{\partial N_1}{\partial t} = -W_{1,2}N_1 + W_{2,1}N_2 + A_{2,1}N_2 + A_{3,1}N_3 - K_{\mathrm{YbTm}}N_1N_8 + K_{\mathrm{TmHo}}N_2N_9 - K_{\mathrm{ErTm31}}N_1N_6 - K_{\mathrm{ErTm21}}N_1N_5 \tag{1k}$$

The transition rates are given by $W_{i,j}(z) = \frac{\sigma_{i,j}(\lambda_{\mathrm{p/s}})}{h\frac{c_0}{\lambda_{\mathrm{p/s}}}} P_{\mathrm{p/s}} \frac{\Gamma_{\mathrm{p/s}}}{A_{\mathrm{d}}}$, where $\sigma_{i,j}(\lambda_{\mathrm{p/s}})$ is the cross section at the wavelength $\lambda_{\mathrm{p/s}}$ pertaining to the $i \to j$ transition, h is the Planck constant, c_0 is the speed of light in vacuum, $\lambda_{\mathrm{p/s}}$ is the pump/signal wavelength, $P_{\mathrm{p/s}}$ is the pump/signal power, $\Gamma_{\mathrm{p/s}}$ is the overlap factor between the doped region and the pump/signal beam profile, and A_{d} is the doped area. The radiative decay rates are given by $A_{i,j} = \frac{\beta_{i,j}}{\tau_i}$, where $\beta_{i,j}$ is the branching ratio pertaining to the $i \to j$ transition, and τ_i is the lifetime of the i-th energy level. The seven parameters K_{ErHo}, K_{ErTm12}, K_{ErTm13}, K_{TmHo}, K_{YbEr}, K_{YbHo}, K_{YbTm} describe the energy transfers between the different rare earth ions. In order to solve the system (1a)–(1k), steady-state conditions are assumed, i.e. $\frac{\partial N_1}{\partial t} = \frac{\partial N_2}{\partial t} = \cdots =$

$\frac{\partial N_{11}}{\partial t} = 0$, and the following conditions are imposed:

$$N_1 + N_2 + N_3 = N_{\text{Tm}}$$
$$N_4 + N_5 + N_6 = N_{\text{Er}}$$
$$N_7 + N_8 = N_{\text{Yb}}$$
$$N_9 + N_{10} + N_{11} = N_{\text{Ho}}$$

where N_{Tm}, N_{Er}, N_{Yb} and N_{Ho} are the thulium, erbium, ytterbium and holmium dopant concentrations, respectively.

The evolution of the pump and signals powers along the fiber is governed by the power propagation equations. In particular, one equation for the pump and six equations for the laser signals (three for each propagation direction) are considered, as follows:

$$\frac{\mathrm{d}P_{\text{p}}}{\mathrm{d}z} = \left[g_{\text{p}}(z) - \alpha(\lambda_{\text{p}})\right] P_{\text{p}}(z) \tag{2a}$$
$$\frac{\mathrm{d}P^{\pm}_{\text{s1}}}{\mathrm{d}z} = \pm\left[g_{\text{s1}}(z) - \alpha(\lambda_{\text{s1}})\right] P^{\pm}_{\text{s1}}(z) \tag{2b}$$
$$\frac{\mathrm{d}P^{\pm}_{\text{s2}}}{\mathrm{d}z} = \pm\left[g_{\text{s2}}(z) - \alpha(\lambda_{\text{s2}})\right] P^{\pm}_{\text{s2}}(z) \tag{2c}$$
$$\frac{\mathrm{d}P^{\pm}_{\text{s3}}}{\mathrm{d}z} = \pm\left[g_{\text{s3}}(z) - \alpha(\lambda_{\text{s3}})\right] P^{\pm}_{\text{s3}}(z) \tag{2d}$$

where $\alpha(\lambda_{\text{p/s}})$ is the optical loss of the glass at the wavelength $\lambda_{\text{p/s}}$, and the gain coefficients are given by:

$$\begin{aligned} g_{\text{p}}(z) &= [-\sigma_{4,6}(\lambda_{\text{p}})N_4(z) + \sigma_{6,4}(\lambda_{\text{p}})N_6(z)]\Gamma_{\text{p}} \\ &\quad + [-\sigma_{7,8}(\lambda_{\text{p}})N_7(z) + \sigma_{8,7}(\lambda_{\text{p}})N_8(z)]\Gamma_{\text{p}}, \\ g_{\text{s1}}(z) &= [-\sigma_{4,5}(\lambda_{\text{s1}})N_4(z) + \sigma_{5,4}(\lambda_{\text{s1}})N_5(z)]\Gamma_{\text{s1}}, \\ g_{\text{s2}}(z) &= [-\sigma_{1,2}(\lambda_{\text{s2}})N_1(z) + \sigma_{2,1}(\lambda_{\text{s2}})N_2(z)]\Gamma_{\text{s2}}, \\ g_{\text{s3}}(z) &= [-\sigma_{9,10}(\lambda_{\text{s3}})N_9(z) + \sigma_{10,9}(\lambda_{\text{s3}})N_{10}(z)]\Gamma_{\text{s3}}. \end{aligned}$$

The pump gain coefficient $g_{\text{p}}(z)$ takes into account the interaction of the pump beam with both erbium and ytterbium ions, as both of them exhibit absorption bands around $\lambda_{\text{p}} = 980$ nm.

The differential equations (2a)–(2d) are solved with the boundary conditions imposed by the input pump and the optical cavity mirrors (see Fig. 1):

$$P_{\text{p}}(0) = P_{\text{p0}}$$
$$P^{+}_{\text{s1}}(0) = R^{\text{in}}_{\text{s1}} P^{-}_{\text{s1}}(0)$$
$$P^{-}_{\text{s1}}(L) = R^{\text{out}}_{\text{s1}} P^{+}_{\text{s1}}(L)$$
$$P^{+}_{\text{s2}}(0) = R^{\text{in}}_{\text{s2}} P^{-}_{\text{s2}}(0)$$
$$P^{-}_{\text{s2}}(L) = R^{\text{out}}_{\text{s2}} P^{+}_{\text{s2}}(L)$$
$$P^{+}_{\text{s3}}(0) = R^{\text{in}}_{\text{s3}} P^{-}_{\text{s3}}(0)$$
$$P^{-}_{\text{s3}}(L) = R^{\text{out}}_{\text{s3}} P^{+}_{\text{s3}}(L)$$

where L is the fiber length, P_{p0} is the input pump power, $R^{\text{in}}_{\text{s1}}$, $R^{\text{in}}_{\text{s2}}$ and $R^{\text{in}}_{\text{s3}}$ are the reflectivities of the three input mirrors at $z = 0$, and $R^{\text{out}}_{\text{s1}}$, $R^{\text{out}}_{\text{s2}}$ and $R^{\text{out}}_{\text{s3}}$ are the reflectivities of the three output mirrors at $z = L$.

TABLE I
SPECTROSCOPIC PARAMETERS FOR THE Tm:Er:Yb:Ho CO-DOPED GERMANATE GLASS

Parameter	Value	Description
$\sigma_{1,2}(\lambda_{\text{s2}})$	1.6×10^{-25} m^2 [21]	Absorption cross section
$\sigma_{2,1}(\lambda_{\text{s2}})$	4.8×10^{-25} m^2 [21]	Emission cross section
$\sigma_{4,5}(\lambda_{\text{s1}})$	2.3×10^{-25} m^2 [22]	Absorption cross section
$\sigma_{5,4}(\lambda_{\text{s1}})$	3.8×10^{-25} m^2 [22]	Emission cross section
$\sigma_{4,6}(\lambda_{\text{p}})$	7×10^{-25} m^2 [23]	Absorption cross section
$\sigma_{6,4}(\lambda_{\text{p}})$	7×10^{-25} m^2 [23]	Emission cross section
$\sigma_{7,8}(\lambda_{\text{p}})$	1.2×10^{-24} m^2 [23]	Absorption cross section
$\sigma_{8,7}(\lambda_{\text{p}})$	1.2×10^{-24} m^2 [23]	Emission cross section
$\sigma_{9,10}(\lambda_{\text{s3}})$	1.25×10^{-25} m^2 [21]	Absorption cross section
$\sigma_{10,9}(\lambda_{\text{s3}})$	4.4×10^{-25} m^2 [21]	Emission cross section
τ_2	2.1 ms [24]	^{3}F$_4$ lifetime
τ_3	1.63 ms [24]	^{3}H$_5$ lifetime
τ_5	10 ms [23]	^{4}I$_{13/2}$ lifetime
τ_6	2 µs [23]	^{4}I$_{11/2}$ lifetime
τ_8	1 ms [23]	^{2}F$_{5/2}$ lifetime
τ_{10}	7.35 ms [24]	^{5}I$_7$ lifetime
τ_{11}	3.52 ms [24]	^{5}I$_6$ lifetime
$\beta_{3,1}$	98.53 % [24]	^{3}H$_5 \rightarrow {}^3$H$_6$ branching ratio
$\beta_{3,2}$	1.47 % [24]	^{3}H$_5 \rightarrow {}^3$F$_4$ branching ratio
$\beta_{6,4}$	≈0 %	^{4}I$_{11/2} \rightarrow {}^4$I$_{15/2}$ branching ratio
$\beta_{6,5}$	≈100 %	^{4}I$_{11/2} \rightarrow {}^4$I$_{13/2}$ branching ratio
$\beta_{11,9}$	19.43 % [24]	^{5}I$_6 \rightarrow {}^5$I$_7$ branching ratio
$\beta_{11,10}$	80.57 % [24]	^{5}I$_6 \rightarrow {}^5$I$_8$ branching ratio
K_{ErHo}	4×10^{-22} m^3 s^{-1} [25]	$Er^{3+} \rightarrow Ho^{3+}$ energy transfer
K_{ErTm12}	4×10^{-22} m^3 s^{-1} [25]	$Er^{3+} \rightarrow Tm^{3+}$ energy transfer
K_{ErTm13}	4×10^{-22} m^3 s^{-1} [25]	$Er^{3+} \rightarrow Tm^{3+}$ energy transfer
K_{TmHo}	4×10^{-22} m^3 s^{-1} [25]	$Tm^{3+} \rightarrow Ho^{3+}$ energy transfer
K_{YbEr}	4×10^{-22} m^3 s^{-1} [25]	$Yb^{3+} \rightarrow Er^{3+}$ energy transfer
K_{YbHo}	4×10^{-22} m^3 s^{-1} [25]	$Yb^{3+} \rightarrow Ho^{3+}$ energy transfer
K_{YbTm}	4×10^{-22} m^3 s^{-1} [25]	$Yb^{3+} \rightarrow Tm^{3+}$ energy transfer

The output powers of the three laser signals and the related efficiencies are calculated as follows:

$$P^{\text{out}}_{\text{s1}} = (1 - R^{\text{out}}_{\text{s1}})P^{+}_{\text{s1}}(L)$$
$$P^{\text{out}}_{\text{s2}} = (1 - R^{\text{out}}_{\text{s2}})P^{+}_{\text{s2}}(L)$$
$$P^{\text{out}}_{\text{s3}} = (1 - R^{\text{out}}_{\text{s3}})P^{+}_{\text{s3}}(L)$$
$$\eta_{\text{s1}} = \frac{P^{\text{out}}_{\text{s1}}}{P_{\text{p0}}}$$
$$\eta_{\text{s2}} = \frac{P^{\text{out}}_{\text{s2}}}{P_{\text{p0}}}$$
$$\eta_{\text{s3}} = \frac{P^{\text{out}}_{\text{s3}}}{P_{\text{p0}}}$$

III. NUMERICAL RESULTS

A step-index fiber, which allows single-mode light propagation for the pump and the three laser signals, is designed. It has a core diameter of $d_{\text{co}} = 4\,\mu$m and a numerical aperture of $NA = 0.17$, with a V-number equal to $V = \frac{2\pi}{\lambda_{\text{p}}}\frac{d_{\text{co}}}{2}NA = 2.18$ at $\lambda_{\text{p}} = 980$ nm. The Tm:Er:Yb:Ho co-doped germanate glass allows a good light confinement along with low optical losses, which are assumed close to $\alpha(\lambda) = 2$ dB m^{-1} as the worst case in the considered pump and signals wavelength range. Its refractive index dispersion is modeled through a Sellmeier equation [20], while Table I reports its spectroscopic parameters.

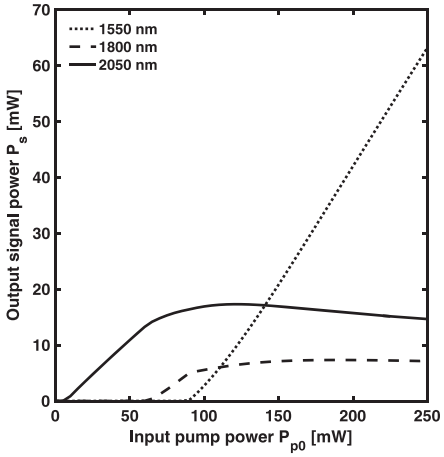

Fig. 3. Output signal power P_s^{out} of the Tm:Er:Yb:Ho fiber laser as a function of the input pump power P_{p0} for the three output wavelengths, $\lambda_{s1} = 1550$ nm (dotted curve), $\lambda_{s2} = 1800$ nm (dashed curve), $\lambda_{s3} = 2050$ nm (solid curve).

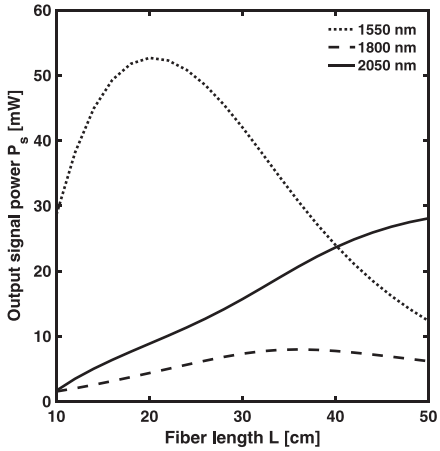

Fig. 4. Output signal power P_s^{out} of the Tm:Er:Yb:Ho fiber laser as a function of the fiber length L for the three output wavelengths, $\lambda_{s1} = 1550$ nm (dotted curve), $\lambda_{s2} = 1800$ nm (dashed curve), $\lambda_{s3} = 2050$ nm (solid curve). Input pump power $P_{p0} = 200$ mW.

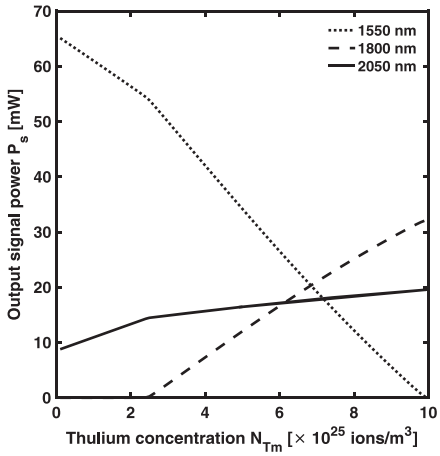

Fig. 5. Output signal power P_s^{out} of the Tm:Er:Yb:Ho fiber laser as a function of the thulium concentration N_{Tm} for the three output wavelengths, $\lambda_{s1} = 1550$ nm (dotted curve), $\lambda_{s2} = 1800$ nm (dashed curve), $\lambda_{s3} = 2050$ nm (solid curve). Input pump power $P_{p0} = 200$ mW.

Values reported in Table I are taken from multiple sources which authors expect to provide a reliable set of parameters. Simulations provide an initial educated guess of optimal condition, a following fine tuning of the optimal laser design could be required and an experimental evaluation of the four-fold doped system [9] is planned in the near future. Nevertheless, the illustrated optimization methodology is based on a general and feasible approach which can be applied to other multi-doped glass systems. The core is uniformly doped with the rare earths. In the simulation, perfectly matched layers (PMLs) are used to avoid reflections of the outgoing waves into the computational domain. Since obtaining laser emission at $\lambda_{s1} = 1550$ nm, $\lambda_{s2} = 1800$ nm and $\lambda_{s3} = 2050$ nm simultaneously with similar power levels is not trivial, preliminary simulations are carried out to determine suitable nominal values for the input parameters, which are the following: $P_{p0} = 200$ mW, $L = 30$ cm, $N_{Tm} = 4 \times 10^{25}$ ions/m^3, $N_{Er} = 3.5 \times 10^{25}$ ions/m^3, $N_{Yb} = 1 \times 10^{25}$ ions/m^3, $N_{Ho} = 4.5 \times 10^{25}$ ions/m^3, $R_{s1}^{in} = R_{s2}^{in} = R_{s3}^{in} = 99\%$ and $R_{s1}^{out} = R_{s2}^{out} = R_{s3}^{out} = 50\%$. A reasonably low input pump power $P_{p0} = 200$ mW is considered in order to avoid detrimental thermal effects. Several parametric sweeps are performed in order to study the behavior of the device. In particular, the laser characteristics are investigated as a function of: i) input pump power P_{p0}, see Fig. 3; ii) fiber length L, see Fig. 4; iii) thulium, erbium, ytterbium and holmium concentrations (N_{Tm}, N_{Er}, N_{Yb}, N_{Ho}), see Figs. 5–8; iv) output mirrors reflectivities (R_{s1}^{out}, R_{s2}^{out}, R_{s3}^{out}), see Figs. 9–11. For each parametric sweep, only one parameter is varied, while all the others are kept constant, i.e. equal to the nominal values.

Fig. 3 shows the dependence of the three output signals with respect to the input pump power. For pump powers up to $P_{p0} = 60$ mW, there is no laser emission at $\lambda_{s1} = 1550$ nm and $\lambda_{s2} = 1800$ nm, but only the signal at $\lambda_{s3} = 2050$ nm is emitted with a slope efficiency equal to $SE_{s3} = 25.6\%$. For pump powers $P_{p0} > 65$ mW, there is also emission at $\lambda_{s2} = 1800$ nm, with a slope efficiency of about $SE_{s2} = 19\%$. The laser threshold to obtain emission also at $\lambda_{s1} = 1550$ nm is equal to $P_{s1}^{th} = 90$ mW. It is worth noting the change of slope efficiency for the $\lambda_{s2} = 1800$ nm and $\lambda_{s3} = 2050$ nm signals due to erbium ions activation.

Fig. 4 shows the dependence of the three output signals with respect to the fiber length L. It can be observed that, for $L > 45$ cm, the power emitted at $\lambda_{s1} = 1550$ nm decreases rapidly, i.e. the curve shows a high negative slope. Conversely, the power emitted at $\lambda_{s3} = 2050$ nm continues to increase. It can be deduced that, as the fiber length is increased beyond $L = 45$ cm, only the emission by the Ho^{3+} ions at $\lambda_{s3} = 2050$ nm is advantaged compared to the other two wavelengths.

Fig. 5 shows the three output signals as functions of the thulium concentration. For low concentrations of thulium, the emission at $\lambda_{s1} = 1550$ nm dominates. The decreasing trend of the power indicates that there is an energy transfer between erbium and thulium ions, even if it is not enough to obtain laser emission at $\lambda_{s2} = 1800$ nm. Laser emission at $\lambda_{s2} = 1800$ nm

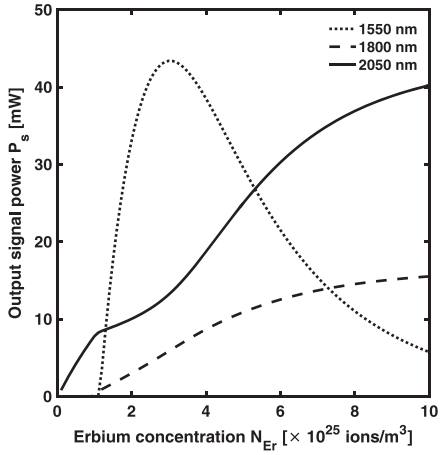

Fig. 6. Output signal power $P_{\mathrm{s}}^{\mathrm{out}}$ of the Tm:Er:Yb:Ho fiber laser as a function of the erbium concentration N_{Er} for the three output wavelengths, $\lambda_{\mathrm{s1}} = 1550$ nm (dotted curve), $\lambda_{\mathrm{s2}} = 1800$ nm (dashed curve), $\lambda_{\mathrm{s3}} = 2050$ nm (solid curve). Input pump power $P_{\mathrm{p0}} = 200$ mW.

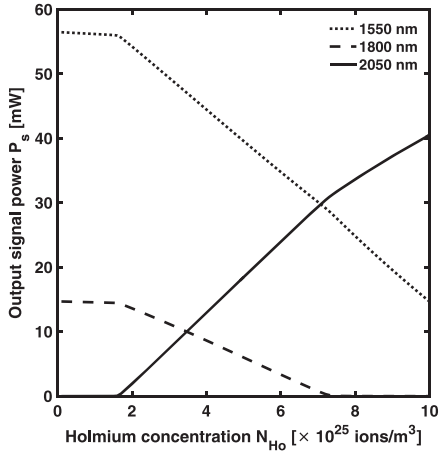

Fig. 8. Output signal power $P_{\mathrm{s}}^{\mathrm{out}}$ of the Tm:Er:Yb:Ho fiber laser as a function of the holmium concentration N_{Ho} for the three output wavelengths, $\lambda_{\mathrm{s1}} = 1550$ nm (dotted curve), $\lambda_{\mathrm{s2}} = 1800$ nm (dashed curve), $\lambda_{\mathrm{s3}} = 2050$ nm (solid curve). Input pump power $P_{\mathrm{p0}} = 200$ mW.

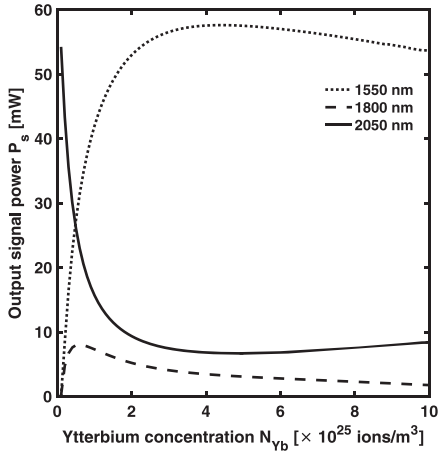

Fig. 7. Output signal power $P_{\mathrm{s}}^{\mathrm{out}}$ of the Tm:Er:Yb:Ho fiber laser as a function of the ytterbium concentration N_{Yb} for the three output wavelengths, $\lambda_{\mathrm{s1}} = 1550$ nm (dotted curve), $\lambda_{\mathrm{s2}} = 1800$ nm (dashed curve), $\lambda_{\mathrm{s3}} = 2050$ nm (solid curve). Input pump power $P_{\mathrm{p0}} = 200$ mW.

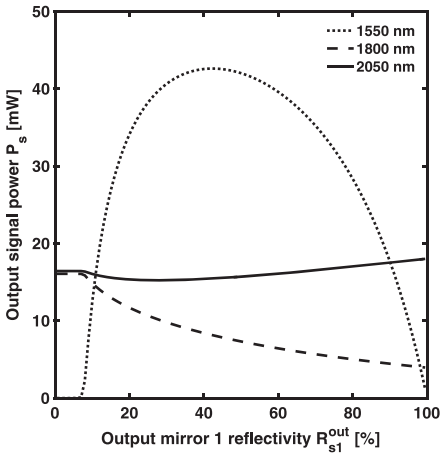

Fig. 9. Output signal power $P_{\mathrm{s}}^{\mathrm{out}}$ of the Tm:Er:Yb:Ho fiber laser as a function of the output mirror 1 reflectivity $R_{\mathrm{s1}}^{\mathrm{out}}$ for the three output wavelengths, $\lambda_{\mathrm{s1}} = 1550$ nm (dotted curve), $\lambda_{\mathrm{s2}} = 1800$ nm (dashed curve), $\lambda_{\mathrm{s3}} = 2050$ nm (solid curve). Input pump power $P_{\mathrm{p0}} = 200$ mW.

starts at the concentration $N_{\mathrm{Tm}} = 2.5 \times 10^{25} \mathrm{ions/m^3}$, at which the other two signals, i.e. $\lambda_{\mathrm{s1}} = 1550$ nm and $\lambda_{\mathrm{s3}} = 2050$ nm, have a negative variation in the slope of their respective curves.

Fig. 6 shows the three output signals as functions of the erbium concentration. For low concentrations of erbium, laser emission occurs only at $\lambda_{\mathrm{s3}} = 2050$ nm. It is observed that the slope of the $\lambda_{\mathrm{s3}} = 2050$ nm signal changes at $N_{\mathrm{Er}} = 1.1 \times 10^{25} \mathrm{ions/m^3}$, for which concentration value laser emission at $\lambda_{\mathrm{s2}} = 1800$ nm starts with a linear increase. By increasing the erbium concentration, only the output powers at $\lambda_{\mathrm{s2}} = 1800$ nm and $\lambda_{\mathrm{s3}} = 2050$ nm increase, while the emission at $\lambda_{\mathrm{s1}} = 1550$ nm, typical of erbium, rapidly drops to few milliwatts. This is due to the energy transfer from the erbium ions to the other rare earths.

Fig. 7 shows the three output signals as functions of the ytterbium concentration. For low ytterbium concentrations, there is a great variability in all the three output signals: the curve at $\lambda_{\mathrm{s1}} = 1550$ nm has an increasing behavior, the curve at $\lambda_{\mathrm{s2}} = 1800$ nm has a maximum of $P_{\mathrm{s2}}^{\mathrm{out}} = 8.04$ mW for $N_{\mathrm{Yb}} = 6 \times 10^{24}$ ions$/\mathrm{m^3}$, and the curve at $\lambda_{\mathrm{s3}} = 2050$ nm has a decreasing behavior. It can be deduced that, with the same pump power at $\lambda_{\mathrm{p}} = 980$ nm, a higher concentration of Yb^{3+} ions produces a greater excitation of Er^{3+} ions, which confirms the strong interaction between the two rare earths.

Fig. 8 shows the three output signals as functions of the holmium concentration. For concentrations less than $N_{\mathrm{Ho}} = 1.7 \times 10^{25}$ ions$/\mathrm{m^3}$, no laser emission at $\lambda_{\mathrm{s3}} = 2050$ nm occurs and the pump excites only the Tm^{3+} and Er^{3+} ions, implying that the system is not affected by the presence of small concentrations of holmium in the glass. Once the holmium concentration of $N_{\mathrm{Ho}} = 1.7 \times 10^{25}$ ions$/\mathrm{m^3}$ has been exceeded, for each further increase the output powers at $\lambda_{\mathrm{s1}} = 1550$ nm and

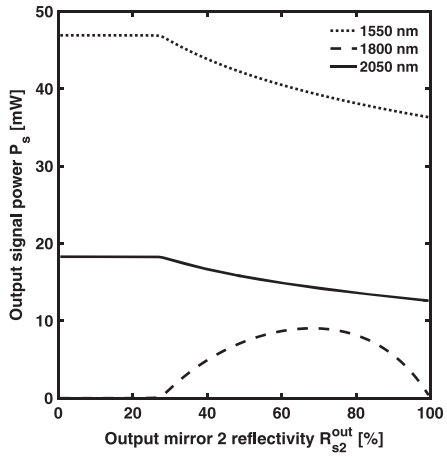

Fig. 10. Output signal power $P_{\rm s}^{\rm out}$ of the Tm:Er:Yb:Ho fiber laser as a function of the output mirror 2 reflectivity $R_{\rm s2}^{\rm out}$ for the three output wavelengths, $\lambda_{\rm s1} = 1550$ nm (dotted curve), $\lambda_{\rm s2} = 1800$ nm (dashed curve), $\lambda_{\rm s3} = 2050$ nm (solid curve). Input pump power $P_{\rm p0} = 200$ mW.

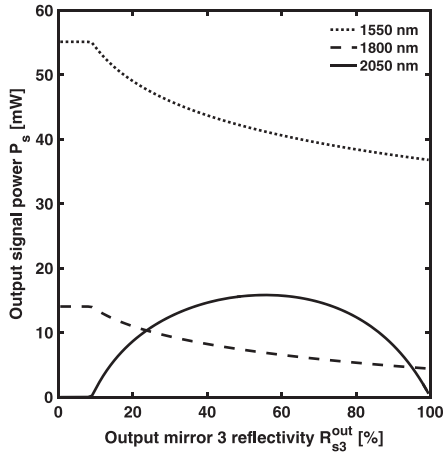

Fig. 11. Output signal power $P_{\rm s}^{\rm out}$ of the Tm:Er:Yb:Ho fiber laser as a function of the output mirror 3 reflectivity $R_{\rm s3}^{\rm out}$ for the three output wavelengths, $\lambda_{\rm s1} = 1550$ nm (dotted curve), $\lambda_{\rm s2} = 1800$ nm (dashed curve), $\lambda_{\rm s3} = 2050$ nm (solid curve). Input pump power $P_{\rm p0} = 200$ mW.

$\lambda_{\rm s2} = 1800$ nm progressively decrease until they reach negligible values.

Fig. 9 shows the three output signals as functions of the output mirror 1 reflectivity $R_{\rm s1}^{\rm out}$. As expected, for small values of $R_{\rm s1}^{\rm out}$, laser emission at $\lambda_{\rm s1} = 1550$ nm cannot occur. The increase of reflectivity beyond $R_{\rm s1}^{\rm out} = 7\%$ results in a reduction of the output power at $\lambda_{\rm s2} = 1800$ nm and a very small variation of the output power at $\lambda_{\rm s3} = 2050$ nm. Therefore, the emission by holmium ions is advantaged with respect to the emission by thulium ions. The curves intersect around $R_{\rm s1}^{\rm out} = 11\%$, for which all the three output signals are close to about $P_{\rm s1}^{\rm out} = P_{\rm s2}^{\rm out} = P_{\rm s3}^{\rm out} = 15$ mW.

Fig. 10 shows the three output signals as functions of the output mirror 2 reflectivity $R_{\rm s2}^{\rm out}$. As in the previous case, for small values of $R_{\rm s2}^{\rm out}$ there is no laser emission at $\lambda_{\rm s2} = 1800$ nm. As the reflectivity is increased beyond $R_{\rm s2}^{\rm out} = 27\%$, laser emission at $\lambda_{\rm s2} = 1800$ nm occurs, and consequently the output powers at $\lambda_{\rm s1} = 1550$ nm and at $\lambda_{\rm s3} = 2050$ nm begin to progressively decrease. It can be observed that, unlike the previous case, an increase of $R_{\rm s2}^{\rm out}$ no longer corresponds to an improvement of the power emitted at $\lambda_{\rm s3} = 2050$ nm.

Fig. 11 shows the three output signals as functions of the output mirror 3 reflectivity $R_{\rm s3}^{\rm out}$. The $\lambda_{\rm s3} = 2050$ nm signal has a low reflectivity threshold equal to $R_{\rm s3}^{\rm out} = 9\%$, for which the power emitted by holmium ions is equal to $P_{\rm s3}^{\rm out} = 0.21$ mW. The signals at $\lambda_{\rm s1} = 1550$ nm and $\lambda_{\rm s2} = 1800$ nm are almost constant for $R_{\rm s3}^{\rm out} < 9\%$, with output powers of $P_{\rm s1}^{\rm out} = 55.1$ mW and $P_{\rm s2}^{\rm out} = 14.1$ mW, respectively. It is apparent that it not possible to obtain three similar output powers.

TABLE II
INPUT PARAMETERS FOR THE PARTICLE SWARM OPTIMIZATION

Parameter	Value	Description
D	4	Solution space dimension
N	40	Number of particles
c_1	1.494	Cognitive parameter
c_2	1.494	Social parameter
w	0.9–0.4 (linear decrease)	Inertial weight
μ_1	10	Penalty parameter
μ_2	10	Penalty parameter
$P_{\rm p0}$	200 mW	Input pump power
L	30 cm	Fiber length
$R_{\rm s1}^{\rm in}$	99 %	Input mirror 1 reflectivity
$R_{\rm s1}^{\rm out}$	50 %	Output mirror 1 reflectivity
$R_{\rm s2}^{\rm in}$	99 %	Input mirror 2 reflectivity
$R_{\rm s2}^{\rm out}$	50 %	Output mirror 2 reflectivity
$R_{\rm s3}^{\rm in}$	99 %	Input mirror 3 reflectivity
$R_{\rm s3}^{\rm out}$	50 %	Output mirror 3 reflectivity

IV. REFINEMENT OF TM:ER:YB:HO LASER VIA PARTICLE SWARM OPTIMIZATION

The results reported in Section III are useful for understanding the behavior of the device with respect to the change of the operating conditions and design parameters. However, they show that achieving three output powers as close as possible is not trivial. To this aim, the particle swarm optimization (PSO) algorithm is exploited. It is a global search technique inspired by the social behavior of a school of fish during the food-searching activity. It is derivative-free and can be adapted for multi-core processing [14], [26]–[28]. A special fitness function F is considered since simply maximizing the sum of the output powers would not yield a unique solution:

$$F = P_{\rm s1}^{\rm out} + P_{\rm s2}^{\rm out} + P_{\rm s3}^{\rm out} - \mu_1 |P_{\rm s1}^{\rm out} - P_{\rm s2}^{\rm out}| - \mu_2 |P_{\rm s1}^{\rm out} - P_{\rm s3}^{\rm out}|$$

Two penalty parameters, μ_1 and μ_2, are provided in order to force the optimization algorithm to discard solutions which exhibit a large distance between the three output powers. Table II reports the values of all the input parameters employed in the PSO optimization. The solution space, which has a dimension $D = 4$, is constituted by the four dopant concentrations. They are varied in the range 1×10^{24} to 1×10^{26} ions/m^3. A set of $N = 40$ particles is considered. Each particle represents a tentative global solution to be updated in the multidimensional solution space. In particular, a particle is a position vector in the four-dimensional space of the dopant concentrations. The fitness function is evaluated in the changing position vector of

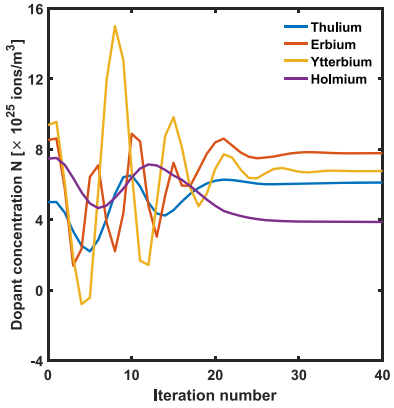

Fig. 12. Dopant concentrations of the Tm:Er:Yb:Ho fiber laser for the 34th particle as a function of the PSO iteration number.

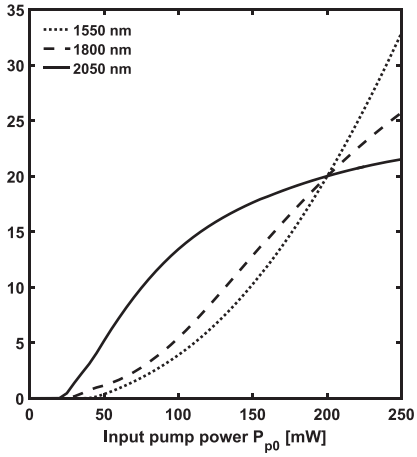

Fig. 13. Output signal power P_s^{out} of the PSO-optimized Tm:Er:Yb:Ho fiber laser as a function of the input pump power P_{p0} for the three output wavelengths, $\lambda_{s1} = 1550$ nm (dotted curve), $\lambda_{s2} = 1800$ nm (dashed curve), $\lambda_{s3} = 2050$ nm (solid curve).

the particles. The algorithm varies the position and the velocity of the particles at each iteration with the aim of maximizing the value of the fitness function. Fig. 12 shows the evolution of the four dopant concentrations for the 34th particle, which corresponds to the best obtained solution, as a function of the PSO iteration number. The optimal Tm:Er:Yb:Ho concentration ratio is found to be $1.58 : 2.01 : 1.75 : 1$, the holmium concentration being $N_{Ho} = 3.87 \times 10^{25}$ ions/m^3. The dependence of the three output signals with respect to the input pump power after the PSO optimization is shown in Fig. 13. The intersection point for $P_{p0} = 200$ mW is apparent, with three output powers equal to $P_{s1}^{out} = 20.01$ mW, $P_{s2}^{out} = 19.99$ mW and $P_{s3}^{out} = 20.02$ mW at $\lambda_{s1} = 1550$ nm, $\lambda_{s2} = 1800$ nm and $\lambda_{s3} = 2050$ nm, respectively. The standard deviation is only $\sigma = 0.008$ mW.

V. Conclusion

For the first time, a novel compact and high efficiency multi-wavelength Tm:Er:Yb:Ho fiber laser is accurately designed and optimized. Simultaneous emission for three different signal wavelengths, $\lambda_{s1} = 1550$ nm, $\lambda_{s2} = 1800$ nm, $\lambda_{s3} = 2050$ nm, can be achieved by pumping at $\lambda_p = 980$ nm. By employing an input pump power of $P_{p0} = 200$ mW with a Tm:Er:Yb:Ho concentration ratio of $1.58 : 2.01 : 1.75 : 1$, the holmium concentration being $N_{Ho} = 3.87 \times 10^{25}$ ions/m^3, output powers of $P_{s1}^{out} = 20.01$ mW, $P_{s2}^{out} = 19.99$ mW and $P_{s3}^{out} = 20.02$ mW at $\lambda_{s1} = 1550$ nm, $\lambda_{s2} = 1800$ nm, $\lambda_{s3} = 2050$ nm, respectively, can be obtained. The three output powers are very close to each other, this confirms that the dopant concentrations can be properly chosen in order to optimize multi-wavelength optical sources or broadband amplifiers which pave the way towards ultrashort pulse emission.

References

[1] M. Eichhorn, "Quasi-three-level solid-state lasers in the near and mid infrared based on trivalent rare earth ions," *Appl. Phys. B*, vol. 93, no. 2, pp. 269–316, Sep. 2008.

[2] A. Hemming, S. D. Jackson, A. Sabella, S. Bennetts, and D. G. Lancaster, "High power, narrow bandwidth and broadly tunable Tm^{3+}, Ho^{3+}-co-doped aluminosilicate glass fibre laser," *Electron. Lett.*, vol. 46, no. 24, pp. 1617–1618, Nov. 2010.

[3] Y. Tian, L. Zhang, S. Feng, R. Xu, L. Hu, and J. Zhang, "2 μm emission of Ho^{3+}-doped fluorophosphate glass sensitized by Yb^{3+}," *Opt. Mater.*, vol. 32, no. 11, pp. 1508–1513, Sep. 2010.

[4] M. Kochanowicz *et al.*, "Analysis of upconversion luminescence in germanate glass and optical fiber codoped with Yb^{3+}/Tb^{3+}," *Appl. Opt.*, vol. 55, no. 9, pp. 2370–2374, Mar. 2016.

[5] J. Zmojda *et al.*, "Investigation of upconversion luminescence in antimony–germanate double-clad two cores optical fiber co-doped with Yb^{3+}/Tm^{3+} and Yb^{3+}/Ho^{3+} ions," *J. Lumin.*, vol. 170, pp. 795–800, Feb. 2016.

[6] J. Zmojda, M. Kochanowicz, P. Miluski, G. C. Righini, M. Ferrari, and D. Dorosz, "Investigation of upconversion luminescence in Yb^{3+}/Tm^{3+}/Ho^{3+} triply doped antimony-germanate glass and double-clad optical fiber," *Opt. Mater.*, vol. 58, pp. 279–284, Aug. 2016.

[7] M. Kochanowicz *et al.*, "Structural and luminescent properties of germanate glasses and double-clad optical fiber co-doped with Yb^{3+}/Ho^{3+}," *J. Alloys Compd.*, vol. 727, pp. 1221–1226, Dec. 2017.

[8] T. Ragin *et al.*, "Enhanced mid-infrared 2.7 μm luminescence in low hydroxide bismuth-germanate glass and optical fiber co-doped with Er^{3+}/Yb^{3+} ions," *J. Non-Cryst. Solids*, vol. 457, pp. 169–174, Feb. 2017.

[9] A. Albalawi, M. Kochanowicz, J. Zmojda, P. Miluski, D. Dorosz, and S. Taccheo, "Fluorescence spectrum of an Yb:Er:Tm:Ho doped germanate glass," in *Proc. Laser Congr. (ASSL)*, Nov. 2018, Art. no. ATu2A.4.

[10] F. Enrichi *et al.*, "Visible to NIR downconversion process in Tb^{3+}-Yb^{3+} codoped silica-hafnia glass and glass-ceramic sol-gel waveguides for solar cells," *J. Lumin.*, vol. 193, pp. 44–50, Jan. 2018.

[11] M. Kochanowicz *et al.*, "Tm^{3+}/Ho^{3+} co-doped germanate glass and double-clad optical fiber for broadband emission and lasing above 2 μm," *Opt. Mater. Express*, vol. 9, no. 3, pp. 1450–1458, Mar. 2019.

[12] L. Sojka *et al.*, "Ultra-broadband mid-infrared emission from a Pr^{3+}/Dy^{3+} co-doped selenide-chalcogenide glass fiber spectrally shaped by varying the pumping arrangement," *Opt. Mater. Express*, vol. 9, no. 5, pp. 2291–2306, May 2019.

[13] M. C. Falconi *et al.*, "Design of an efficient pumping scheme for mid-IR Dy^{3+}:$Ga_5Ge_{20}Sb_{10}S_{65}$ PCF fiber laser," *IEEE Photon. Technol. Lett.*, vol. 28, no. 18, pp. 1984–1987, Sep. 2016.

[14] M. C. Falconi *et al.*, "Dysprosium-doped chalcogenide master oscillator power amplifier (MOPA) for mid-IR emission," *J. Lightw. Technol.*, vol. 35, no. 2, pp. 265–273, Jan. 2017.

[15] G. Palma *et al.*, "Design of praseodymium-doped chalcogenide micro-disk emitting at 4.7 μm," *Opt. Express*, vol. 25, no. 6, pp. 7014–7030, Mar. 2017.

[16] M. C. Falconi, D. Laneve, M. Bozzetti, T. T. Fernandez, G. Galzerano, and F. Prudenzano, "Design of an efficient pulsed Dy^{3+}:ZBLAN fiber laser operating in gain switching regime," *J. Lightw. Technol.*, vol. 36, no. 23, pp. 5327–5333, Dec. 2018.

[17] M. Shen *et al.*, "Modeling of resonantly pumped mid-infrared Pr^{3+}-doped chalcogenide fiber amplifier with different pumping schemes," *Opt. Express*, vol. 26, no. 18, pp. 23 641–23 660, Sep. 2018.

[18] S. Sujecki *et al.*, "Experimental and numerical investigation to rationalize both near-infrared and mid-infrared spontaneous emission in Pr^{3+} doped selenide-chalcogenide fiber," *J. Lumin.*, vol. 209, pp. 14–20, May 2019.
[19] S. Sujecki *et al.*, "Spatiotemporal modeling of mid-infrared photoluminescence from terbium(III) ion doped chalcogenide-selenide multimode fibers," *J. Rare Earths*, vol. 37, no. 11, pp. 1157–1163, Nov. 2019.
[20] H. T. Munasinghe *et al.*, "Lead-germanate glasses and fibers: A practical alternative to tellurite for nonlinear fiber applications," *Opt. Mater. Express*, vol. 3, no. 9, pp. 1488–1503, Sep. 2013.
[21] Q. Lin, H. Xia, Y. Zhang, J. Wang, J. Zhang, and S. He, "Gain properties of germanate glasses singly doped with Tm^{3+} and Ho^{3+} ions," *J. Rare Earths*, vol. 27, no. 1, pp. 76–82, Feb. 2009.
[22] T. Wei *et al.*, "Mid-infrared fluorescence, energy transfer process and rate equation analysis in Er^{3+} doped germanate glass," *Sci. Rep.*, vol. 4, Aug. 2014, Art. no. 6060.
[23] S. Taccheo, G. Sorbello, S. Longhi, and P. Laporta, "Measurement of the energy transfer and upconversion constants in Er–Yb-doped phosphate glass," *Opt. Quant. Electron.*, vol. 31, no. 3, pp. 249–262, Mar. 1999.
[24] C. A. Evans, Z. Ikonic, B. Richards, P. Harrison, and A. Jha, "Numerical rate equation modeling of a $\sim$2.1–μm–Tm^{3+}/Ho^{3+} co-doped tellurite fiber laser," *J. Lightw. Technol.*, vol. 27, no. 19, pp. 4280–4288, Oct. 2009.
[25] C. Jiang and W. Xu, "Theoretical model of Yb^{3+}-Er^{3+}-Tm^{3+}-codoped system for white light generation," *IEEE/OSA J. Display Technol.*, vol. 5, no. 8, pp. 312–318, Aug. 2009.
[26] G. Palma *et al.*, "Modeling of whispering gallery modes for rare earth spectroscopic characterization," *IEEE Photon. Technol. Lett.*, vol. 27, no. 17, pp. 1861–1863, Sep. 2015.
[27] G. Palma *et al.*, "Novel double step approach for optical sensing via microsphere WGM resonance," *Opt. Express*, vol. 24, no. 23, pp. 26 956–26 971, Nov. 2016.
[28] D. Laneve *et al.*, "Electromagnetic design of microwave cavities for side-coupled linear accelerators: A hybrid numerical/analytical approach," *IEEE Trans. Nucl. Sci.*, vol. 65, no. 8, pp. 2233–2239, Aug. 2018.

Mario Christian Falconi (Student Member, IEEE) received the M.Sc. degree in electronic engineering (*cum laude*) and the Ph.D. degree in electrical and information engineering, both from the Polytechnic University of Bari, Bari, Italy, in 2015 and 2019, respectively. He is currently a Research Fellow with the Polytechnic University of Bari. His research interests include fiber lasers and amplifiers, photonic crystal fibers, and nonlinear effects in optical fibers.

Dario Laneve received the M.Sc. degree in information engineering (*cum laude*) in 2014 from the Polytechnic University of Bari, Bari, Italy, where he is currently working toward the Ph.D. degree in electrical and information engineering. His research interests include microwave resonators for linear accelerators and optical resonators for sensing applications.

Vincenza Portosi received the M.Sc. degree in electronic engineering (*cum laude*) from the Polytechnic University of Bari, Bari, Italy, in 2018. She is currently a Research Fellow with the Polytechnic University of Bari. Her research interests include microwave applicators for medical applications, metamaterials, SIW antennas, and optical fiber sensors.

Stefano Taccheo received the Ph.D. degree in optics-material physics from Politecnico di Milano, Milano, Italy, in 1994. He is currently an Associate Professor with Swansea University, Swansea, U.K. From 2003 to 2007, he was with Politecnico di Milano, Italy. He has authored or coauthored more than 100 journals and conference papers. His research interests include lasers, nonlinear optics, and supercontinuum spectrum generation.

Francesco Prudenzano received the Ph.D. degree in electronic engineering from the Polytechnic University of Bari, Bari, Italy, in November 1996. Since 2018, he has been a Full Professor in Electromagnetic Fields with the Department of Electrical and Information Engineering, Polytechnic University of Bari, Bari, Italy. His research activity regards the design and characterization of microwave devices, integrated optics and optical fiber-based devices. He is the Head of Microwave and Optical Engineering group, Department of Electrical and Information Engineering, Polytechnic University of Bari. From 2017 to 2018, he was the Chair of SIOF, the Italian Society of Optics and Photonics (Italian branch of EOS - European Optical Society). He is involved in several national and international research projects and cooperations. He has coauthored more than 400 publications, 295 of which got published in journals and international conferences, lectures, and invited papers.